

Electronic supplementary information

Environmental context determines the impact of titanium oxide and silver nanoparticles on the functioning of intertidal microalgal biofilms

Claire Passarelli, Xianjin Cui, Eugenia Valsami-Jones, Graham JC Underwood

Fig. S1: Experimental mesocosms shown at “low tide” (top picture) and “high tide” (bottom picture). Experimental tanks (upper shelf) contained sediment cores, while the reservoir tank (on ground) only contained seawater. Sediment cores were 6.8 cm in diameter and 10 cm deep; each tank contains approximately 10 l of seawater.



Supplementary material S2: characterisation of the nanoparticles (method and results).

A – Shape and size

Method

The morphology and size of NPs used in the experiments were characterised by Transmission Electron Microscopy (TEM). TEM grids were prepared by drying 20 μ l of freshly made solution of Ag-NPs or TiO₂-NPs in Ultra-High Purity water on a 300 Mesh copper grid with a holey carbon support film. TEM images were recorded on a JEOL2100F transmission electron microscope operating at 200 kV (field emission electron gun source, information limit 0.19 nm) at the Nanoscale and Microscale Research Centre, University of Nottingham.

Results

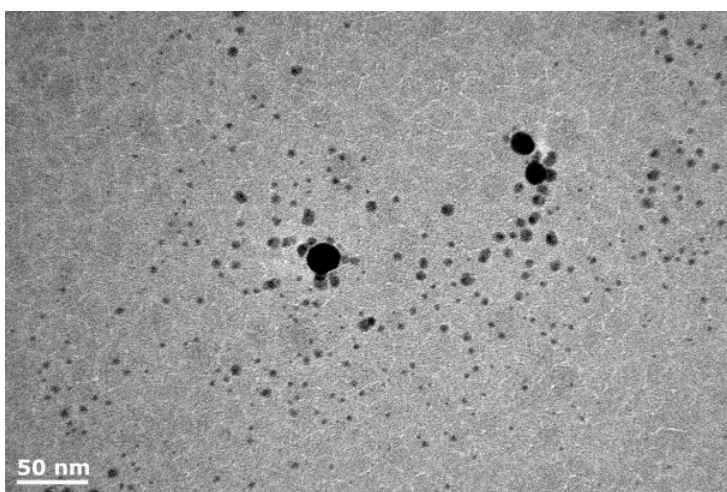


Fig. S2a: typical bright field TEM image of the Ag-NPs used in the experiment. Ag-NPs were well dispersed and exhibited a quasi-spherical shape.

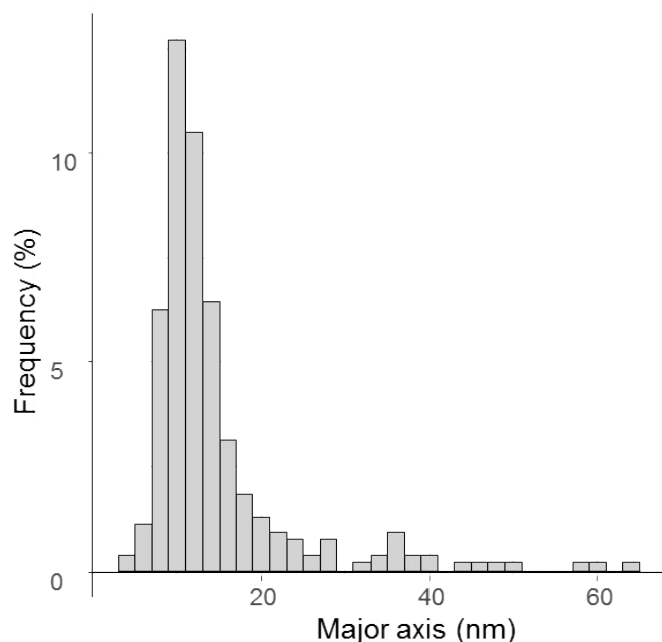


Fig. S2b. Size distribution of Ag-NPs as determined by TEM. Median size was around 12 nm (major axis; 271 NPs were measured).

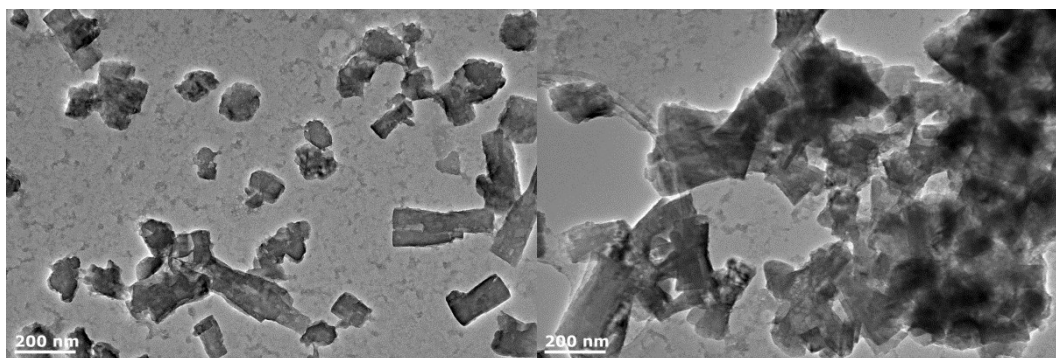


Fig. S2c: Typical bright field TEM images of TiO₂-NPs used in the experiment. TiO₂-NPs had highly irregular shapes and sizes, and aggregated in water. Most individual particles had length and width between 50 and 200 nm.

B – Hydrodynamic diameter of NPs

Method

The hydrodynamic size and Zeta potential of Ag-NPs was characterised by Dynamic Light Scattering (DLS) in *early spring* and *summer* seawaters at a concentration of 3.6 g.l⁻¹ of Ag-NPs, at 8 °C for *early spring* and 22 °C for *summer*. Hydrodynamic size was measured on a Zetasizer Nano ZS ZEN 3600 from Malvern with a scattering angle of 173 degree.

Zeta potential of TiO₂ and Ag-NPs were measured in a dispersion in Ultra-High Purity water with pH = 7.

Results

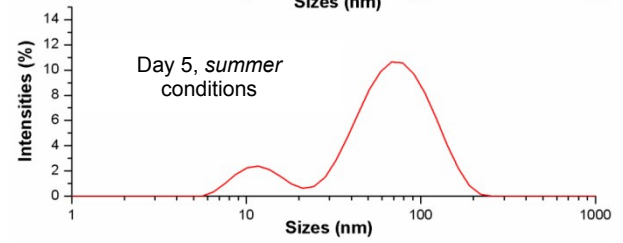
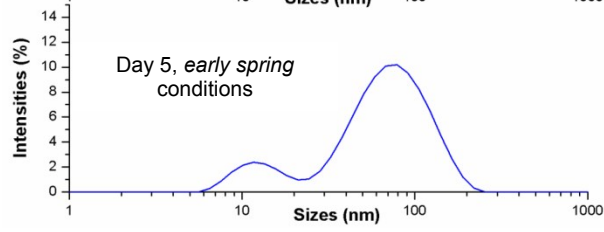
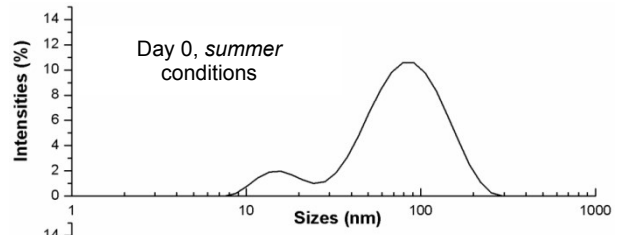
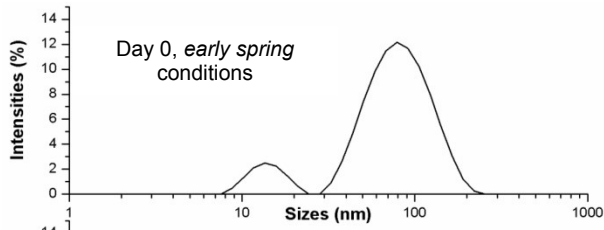


Fig. S2d: Dynamix Light Scattering (DLS) measurements of Ag-NPs. Note that intensities do not reflect the number of particles from each size, with over 90 % of particles belonging to the first peak (smaller size). In both seasons, measurements confirm a majority of particles with hydrodynamic diameter between 10 and 20 nm, and another peak of particles with a larger diameter, around 60-80 nm. After 5 days in seawater, both distributions shifted towards smaller size, due to dissolution of Ag-NPs.

A negative zeta potential was found for both NPs in a neutral environment. TiO₂-NPs exhibited a negative zeta potential of -17.5 ± 0.9 mV, lower than -30 mV at which the dispersion system can be considered as stable. An even lower colloidal stability of TiO₂-NPs in seawater is possible due to the very high ionic strength of seawater. Despite a lower magnitude in zeta potential than TiO₂ (-9 mV vs -17.5mV), Ag-NPs showed a high colloidal stability even in seawater because of the PVP coating. No aggregation was observed by naked eyes or DLS after being kept at room temperature for 5 days. The plasmonic fluorescence of Ag-NPs is sensitive to the particle size and aggregation state. However, no wavelength shift was observed on UV-Vis spectrum for Ag-NPs even after 5 days, showing the absence of aggregation.

C- Dissolution of Ag-NPs

Method:

PVP-coated Ag-NPs were dissolved in 50 ml of *early spring* and *summer* seawater to achieve a stock solution with a concentration of 250 mg.l⁻¹. Five ml of stock solution was immediately diluted to 50 ml with Ultra-High Purity water to make working solutions. Solutions with *summer* seawater were kept covered at room temperature (22 °C), while these with *early spring* seawater solutions were kept at 5 °C, to mimic the temperature-related dissolution conditions at different seasons. 10 ml was taken from the Ag-NPs working solutions at 24 h and 48 h and

filtered by a centrifugal filter with a cut-off size of 10 kDa (Amicon Ultra-15). The concentrations of ionic silver in the filtered solution was measured by ICP-MS (NixION™ 300X from Perkin Elmer). Initial concentration of Ag (both Ag-NPs and ionic Ag) in stock or diluted solutions were also determined by ICP-MS, after digestion with concentrated nitric acid.

Results:

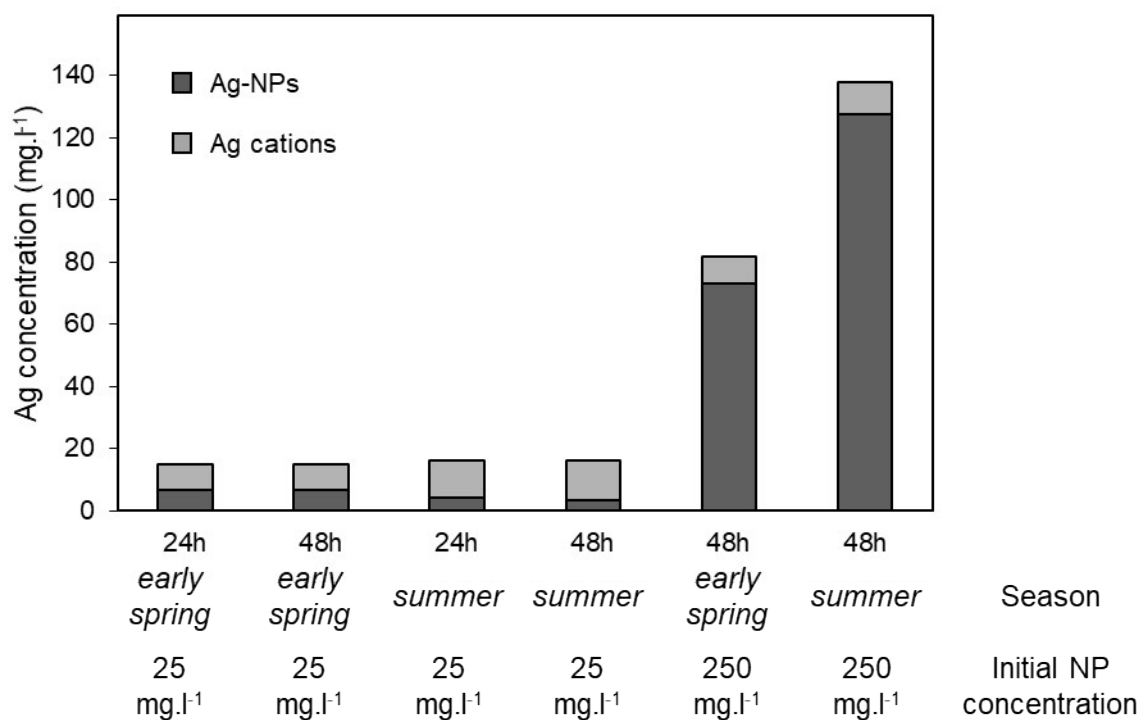
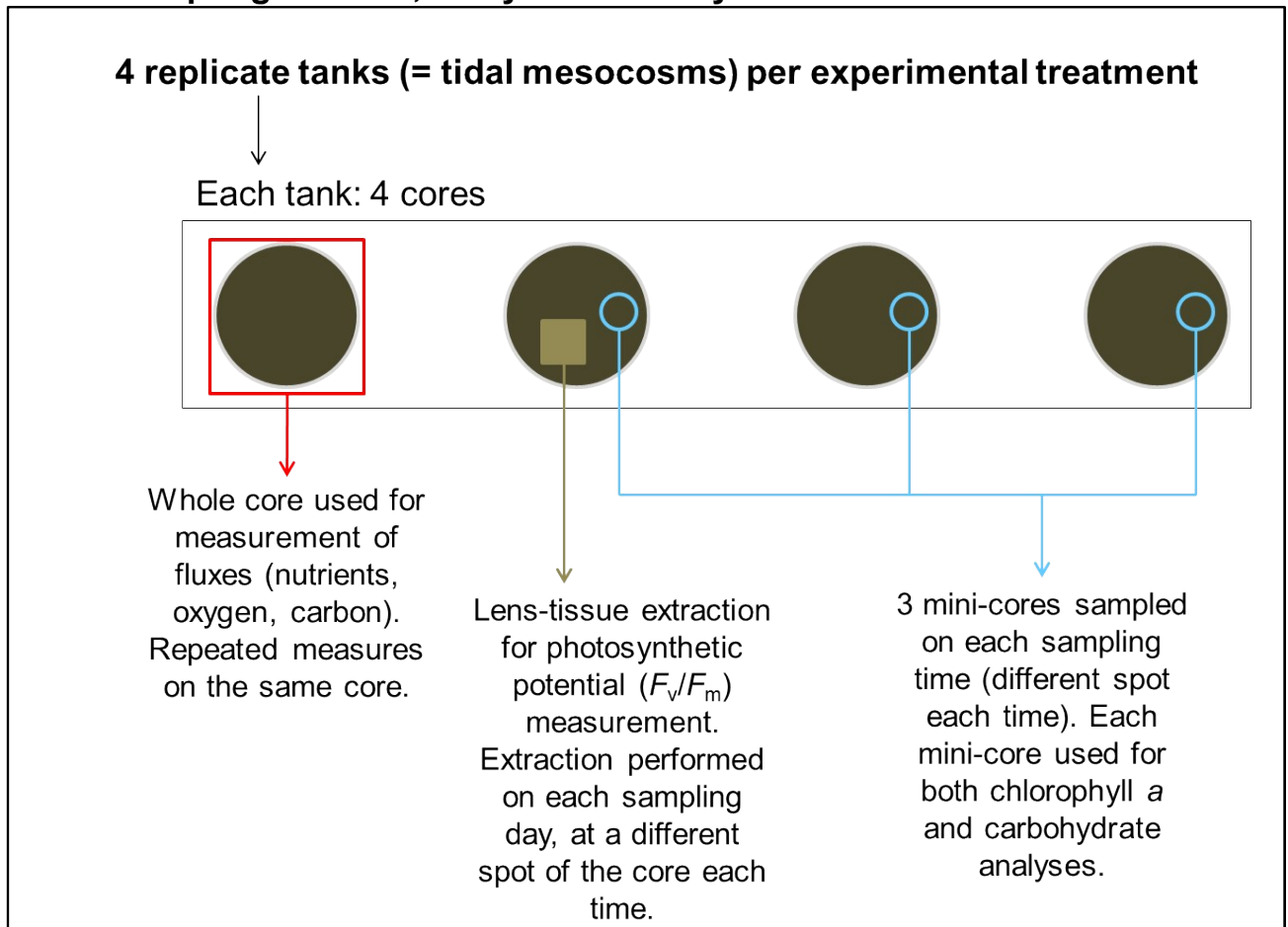


Fig. S2e: ICP-MS results showing the dissolution of PVP coated Ag-NPs in *early spring* seawater (5 °C) and *summer* seawater (22 °C) at different time points (24 h and 48 h), and at different concentration conditions (25 mg.l⁻¹ and 250 mg.l⁻¹). Dissolution was higher in *summer* conditions, and did not increase after 24 h or when initial concentration of NPs exceeded 25 mg.l⁻¹. Note that, due to analytical requirements, the concentrations of silver used for this dissolution study are higher compared to those used in our experiments. Ag total concentration (as determined by ICP-MS) is lower than concentration of PVP-coated Ag-NPs due to the mass of the PVP coating.

Fig. S3: sampling protocol during the experiments. Individual replicate cores were 6.8 cm in diameter. Mini-cores (1.4 cm diameter, 2 mm deep) were taken within larger cores with a cut-off syringe. Lens-tissue extracts were sampled on the larger cores just after emersion (1-hour extraction under light).

Each sampling time: T0, 4 days and 28 days



Supplementary material S4: characterisation of macrofaunal communities.

Visual observation of TiO₂-NPs showed that TiO₂-NPs accumulated at the surface of the sediment, with no visible transport to deeper parts of the cores (see white layer on plate 1 below). However, when removing the core at the end of the experiment, we observed that annelid worm burrows in TiH treatments were lined with TiO₂-NPs (see plate 2); indicating that annelid activity at the surface of the cores transported NPs towards deeper parts of the cores.

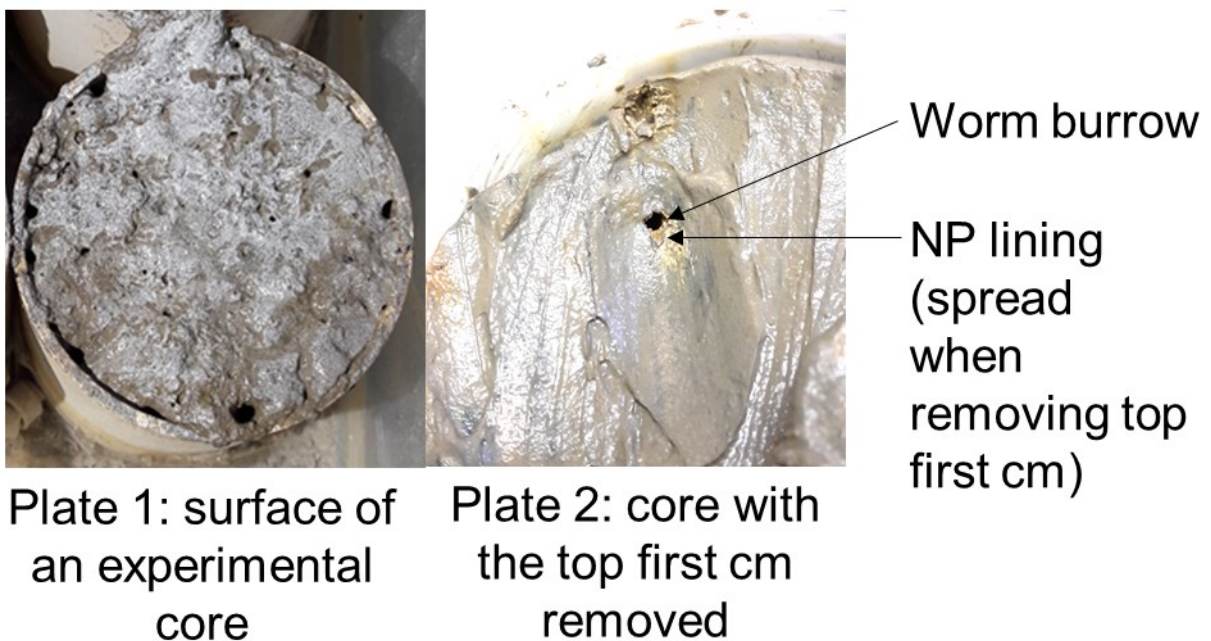
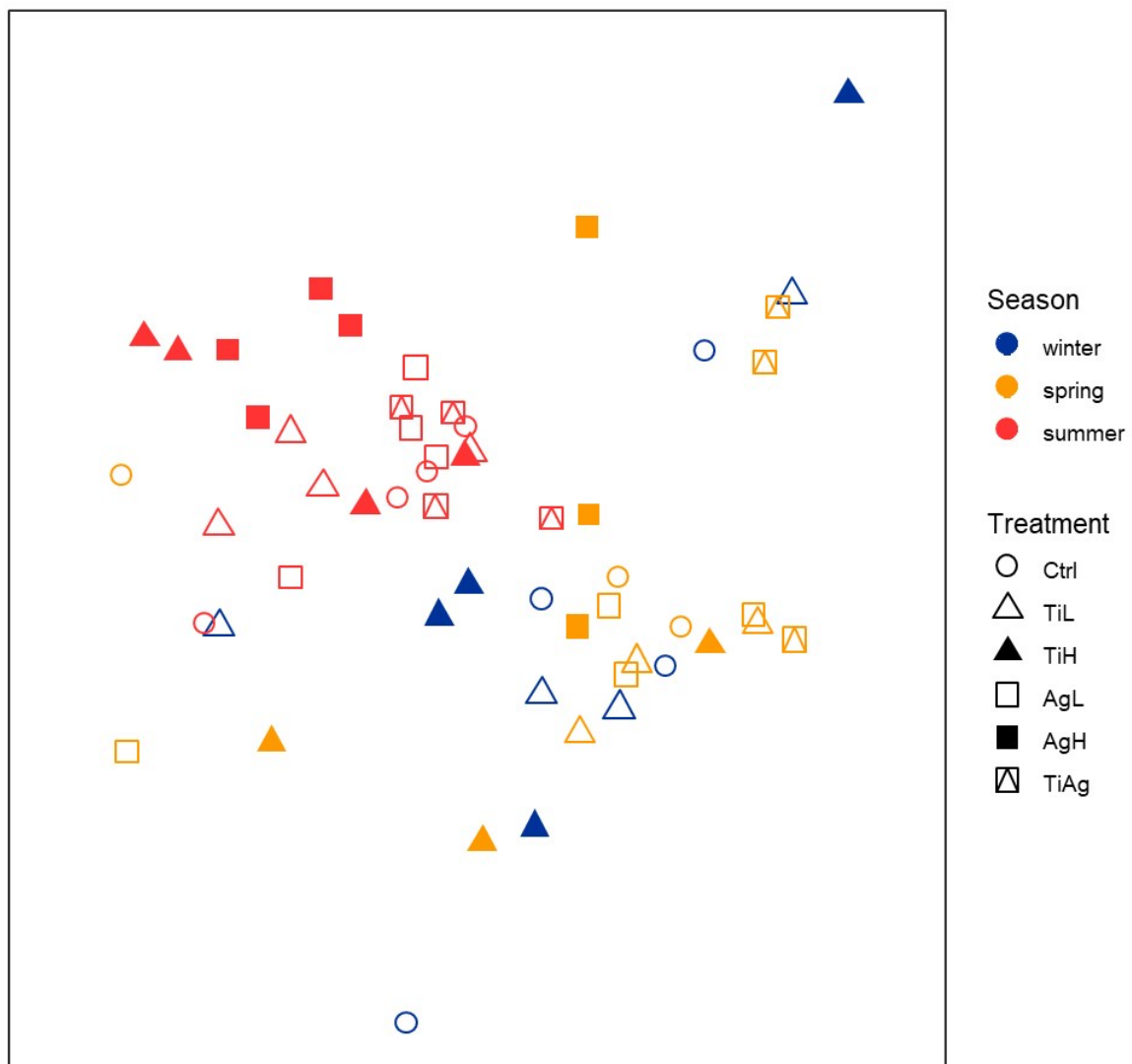


Fig. S4a: The physical accumulation of TiO₂-NPs at the surface of the cores and inside worm tubes in TiH treatments.

To determine if there were any differences in macrofaunal assemblages between treatments and seasons, all cores were sieved for macrofauna (1 mm mesh size) at the end of the experiments, with macrofauna identified, counted and sizes measured. Using published morphometric ratios¹⁻³, we calculated total biovolume of each species and the overall

macrofaunal biovolume for all cores. Within each season, the total macrofauna biovolume did not change significantly between treatments. Therefore, if transport of NPs towards the bottom of the cores significantly altered nanoparticle loads, these alterations were similar between treatments. The abundance of *Hediste diversicolor* was significantly reduced in the TiO₂-NP treatments in the *early spring* experiment.

The macrofaunal community composition in our cores was different between seasons (ANOSIM, R = 0.61, p = 0.001; nMDS of the macrofaunal biovolume data, Fig S4b below): higher densities of *Hediste diversicolor* were present during summer (Table S4c). Therefore, our environmental context encompasses abiotic variables (Table 1), biofilm variables (Table 2) and macrofaunal variables (Fig S4b and Table S4c below).



Stre

Fig. S4b: nMDS plots based on macrofaunal biovolume after 28 days of experiment in all three seasons. C: control, no NP. TiL: target concentration 25 $\mu\text{g.l}^{-1}$ of $\text{TiO}_2\text{-NP}$. TiH: target concentration 25 mg.l^{-1} of $\text{TiO}_2\text{-NP}$. AgL: target concentration 25 ng.l^{-1} of Ag-NP. AgH: target concentration 25 $\mu\text{g.l}^{-1}$ of Ag-NP. TiAg: target concentrations 25 $\mu\text{g.l}^{-1}$ of $\text{TiO}_2\text{-NP}$ and 25 ng.l^{-1} of Ag-NP.

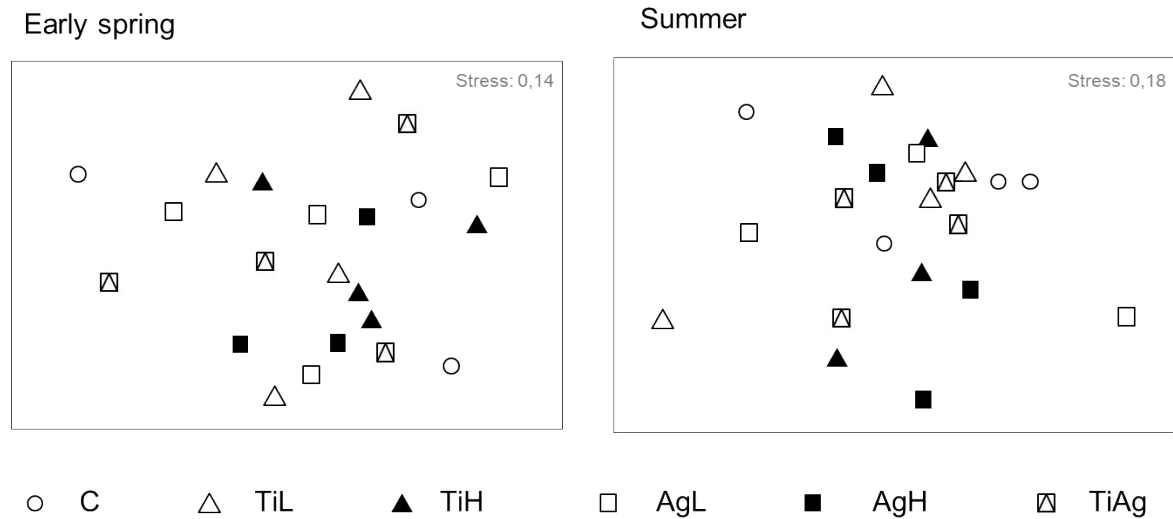
Table S1: Density of macro-invertebrates (individuals.m⁻² \pm se). Significant differences in density between seasons indicated by superscript (a, b, $p < 0.01$ or less, Kruskal-Wallis test). There were no significant treatment effects on individual taxa within seasons except with *Hediste diversicolor* in the *early spring* experiment ($p < 0.05$).

Season (context)	<i>early spring</i>	<i>summer</i>	<i>winter</i>
Taxon	Feb./Mar. 2017 n=19	Jun./Jul. 2017 n=24	Nov./Dec. 2016 n=12
<i>Peringia ulvae</i> (Mollusca, Gastropoda)	1376.7 \pm 163.1	2088.1 \pm 220.5	2019.2 \pm 434.4
<i>Macoma balthica</i> (Mollusca, Bivalvia)	608.7 ^a \pm 122.0	1330.9 ^b \pm 212.0	1170.3 ^b \pm 189.0
<i>Nephtys hombergi</i> (Annelida, Polychaeta)	14.5 \pm 14.5	0.0 \pm 0	45.9 \pm 30.9
<i>Hediste diversicolor</i> (Annelida, Polychaeta)	246.4 ^a \pm 51.1	3327.2 ^b \pm 196.8	298.3 ^a \pm 137.5
C	367.1 ^b \pm 91.8		
TiL	183.6 ^a \pm 91.8		
TiH	0.0 ^a \pm 0.0		
AgL	206.5 ^{a,b} \pm 68.8		
AgH	550.7 ^b \pm 159.0		
TiAg	183.6 ^a \pm 91.8		
Dolicopodid larvae (Arthropoda, Insecta)	43.5 ^a \pm 23.7	0.0 ^b \pm 0	68.8 ^a \pm 36.0
Ostracoda (Arthropoda, Crustacea)	58.0 \pm 33.8	114.7 \pm 32.8	23.0 \pm 23.0

Table S2: fluxes of TOC and inorganic nutrients in the dark (shaded) and in the light at the start of each experiment (mean \pm se, n = 12). A positive flux is a net flux from sediment to seawater.

Season (context)	<i>Early spring</i>	<i>Summer</i>	<i>Winter</i>
Variable	Feb./Mar. 2017	Jun./Jul. 2017	Nov./Dec. 2016
TOC flux in the dark (mg C.m ⁻² .h ⁻¹)	-172 \pm 144	21.8 \pm 24.9	724 \pm 284
TOC flux in the light (mg C.m ⁻² .h ⁻¹)	-409 \pm 110	435 \pm 237	670 \pm 135
NO ₂ ⁻ flux in the dark (μ mol.m ⁻² .h ⁻¹)	-2.3 \pm 0.6	2.3 \pm 1.3	7.9 \pm 4.7
NO ₂ ⁻ flux in the light (μ mol.m ⁻² .h ⁻¹)	-0.58 \pm 0.56	2.0 \pm 1.5	4.6 \pm 1.7
NO ₃ ⁻ flux in the dark (μ mol.m ⁻² .h ⁻¹)	-181 \pm 13.0	-163.4 \pm 16.6	-231 \pm 28.6
NO ₃ ⁻ flux in the light (μ mol.m ⁻² .h ⁻¹)	-74.1 \pm 8.0	-58.9 \pm 9.0	-111 \pm 15.8
NH ₄ ⁺ flux in the dark (μ mol.m ⁻² .h ⁻¹)	-9.6 \pm 18.1	395 \pm 118	62.9 \pm 48.8
NH ₄ ⁺ flux in the light (μ mol.m ⁻² .h ⁻¹)	41.3 \pm 17.7	201 \pm 66.7	30.2 \pm 23.1
SiO ₄ ⁴⁻ flux in the dark (μ mol.m ⁻² .h ⁻¹)	-40.2 \pm 16.9	67.1 \pm 21.6	30.3 \pm 17.2
SiO ₄ ⁴⁻ flux in the light (μ mol.m ⁻² .h ⁻¹)	-60.4 \pm 14.6	54.0 \pm 19.8	11.9 \pm 17.2
PO ₄ ³⁻ flux in the dark (μ mol.m ⁻² .h ⁻¹)	-1.0 \pm 1.2	51.0 \pm 6.4	-8.3 \pm 4.2
PO ₄ ³⁻ flux in the light (μ mol.m ⁻² .h ⁻¹)	5.5 \pm 1.6	33.8 \pm 3.6	-9.2 \pm 3.7

Fig. S5: nMDS plots based on nutrient fluxes between sediment and water after 28 days of experiment in *early spring* and *summer*. C: control, no NP. TiL: target concentration 25 $\mu\text{g.l}^{-1}$ of $\text{TiO}_2\text{-NP}$. TiH: target concentration 25 mg.l^{-1} of $\text{TiO}_2\text{-NP}$. AgL: target concentration 25 ng.l^{-1} of Ag-NP. AgH: target concentration 25 $\mu\text{g.l}^{-1}$ of Ag-NP. TiAg: target concentrations 25 $\mu\text{g.l}^{-1}$ of $\text{TiO}_2\text{-NP}$ and 25 ng.l^{-1} of Ag-NP.



References

1. C. Casagrande and C. F. Boudouresque, A sieving method for rapid determination of size-frequency distribution of small-gastropods. Example of the mud snail *Hydrobia ventrosa* (Gastropoda: Prosobranchia), *Hydrobiologia*, 2002, **485**, 143-152.
2. G. Ejdung, E. Flach, L. Byrén and H. Hummel, Predation by crustaceans on native and non-native Baltic clams, *Aquat. Biol.*, 2009, **6**, 15-24.
3. P. Esselink and L. Zwarts, Seasonal trend in burrow depth and tidal variation in feeding activity of *Nereis diversicolor*, *Mar. Ecol. Prog. Ser.*, 1989, **56**, 243-254.